【論　文】

파형단면을 가진 유하식 집열기의 이론 및 실험 연구

An Experimental And Theoretical Study on the Corrugated Water-Trickle Collector

이 종 호* 정　모** 박 원 훈***
Jong Ho Lee　Mo Chung　Won Hoon Park

초　　록

파형 단면을 가진 유하식 집열기의 이론 및 실험 결과로서 유량, 각도등 집열성능에 미치는 영향등이 고려되었다. 입구 온도와 출구온도 차이가 적을 경우에는 이론과 실험치가 잘 맞으나 온도차이가 많을 경우 혹은 입구온도가 높을 때에는 투과체안에 생기는 결로 및 수증기의 영향으로 편차가 커진다.
개방회로와 폐쇄회로의 경우를 구분하여 실험되었는데 개방회로의 경우 효율은 약간 저하되지만 전반적인 성능은 폐쇄회로와 같은 경향을 나타내었다. 개방회로는 과열을 막는 방편으로 이용될 수 있다.

1. INTRODUCTION

A distinct advantage of the trickle collector over other types of liquid systems is that it is self-draining and therefore does not require either an expensive antifreeze solution or a complex control system. It is an open, non-pressurized system which minimizes expensive and sophisticated plumbing. Although there are certain problems involved in the construction details of a trickle collector, all the necessary principles are easily understood. The required components are widely available and relatively inexpensive.

Even though there are many published reports and studies on the typical flat plate collectors, articles and reports on trickle collectors are uncommon.

San Martin[1] presented the results of outdoor thermal performance testing of three solar energy collectors, including a water-trickle solar collector. The results showed that the water-trickle collector had lower collection efficiencies than the other two collectors. The data displayed collector efficiency as a function of time and do not include incident solar energy values.

Smith[2] reviewed the development of numerical modeling of water-trickle solar collectors, which he related to the experimental work of San Martin.

Bush[3] evaluated a home solar heating system which included a water-trickle collector of his own design. This report included analytical and experimental studies of collector efficiency as a function of collector temperature as well as a function of the difference between collector and ambient temperatures.

Beard *et al.*[4–6] studied the thermal performance of the Thomason "Solaris" water-trickle solar collector. This study included the effects on performance caused by design modifications, such as flow rate variations, the addition of a second glazing, different glazing materials and varying the distance of the glazing(s) from the collector surface. Simulation models were also developed, which included provisions for energy transfer by evaporation and condensation, as well as the customary heat transfer by radiation, convection and conduction.

May[7] presented a solution of the heat and mass transfer equations using a thermal network model to represent the Thomason Solaris collector. The solution of the model, using a digital computer, yielded the steady-state efficiency of the collector as a function of collector configuration, ambient conditions and inlet water temperature.

An experimental and theoretical study of a corrugated steel sheet solar water heater was presented by Wang Shing-An[8]. Even though the collector was not a trickle collector the absorber was con-

*　正會員：韓國動力資源研究所
**　韓國動力資源研究所
***　正會員：科學技術院

structed by soldering two galvanised iron sheets together.

The theoretical part of this paper is devoted to the analysis of the thermal performance of a sinusoidally corrugated trickle water collector. The experimental study was performed to confirm the theoretical analysis and to determine if there were some unexpected phenomena in the collector when the collector was idle or when a considerable temperature rise occurred.

2. THEORETICAL ANALYSIS

The absorber model selected for the numerical analysis is shown in Fig. 1. The analysis of a corrugated trickle collector is more complex than that of flat plate due to the fact that the absorber is not

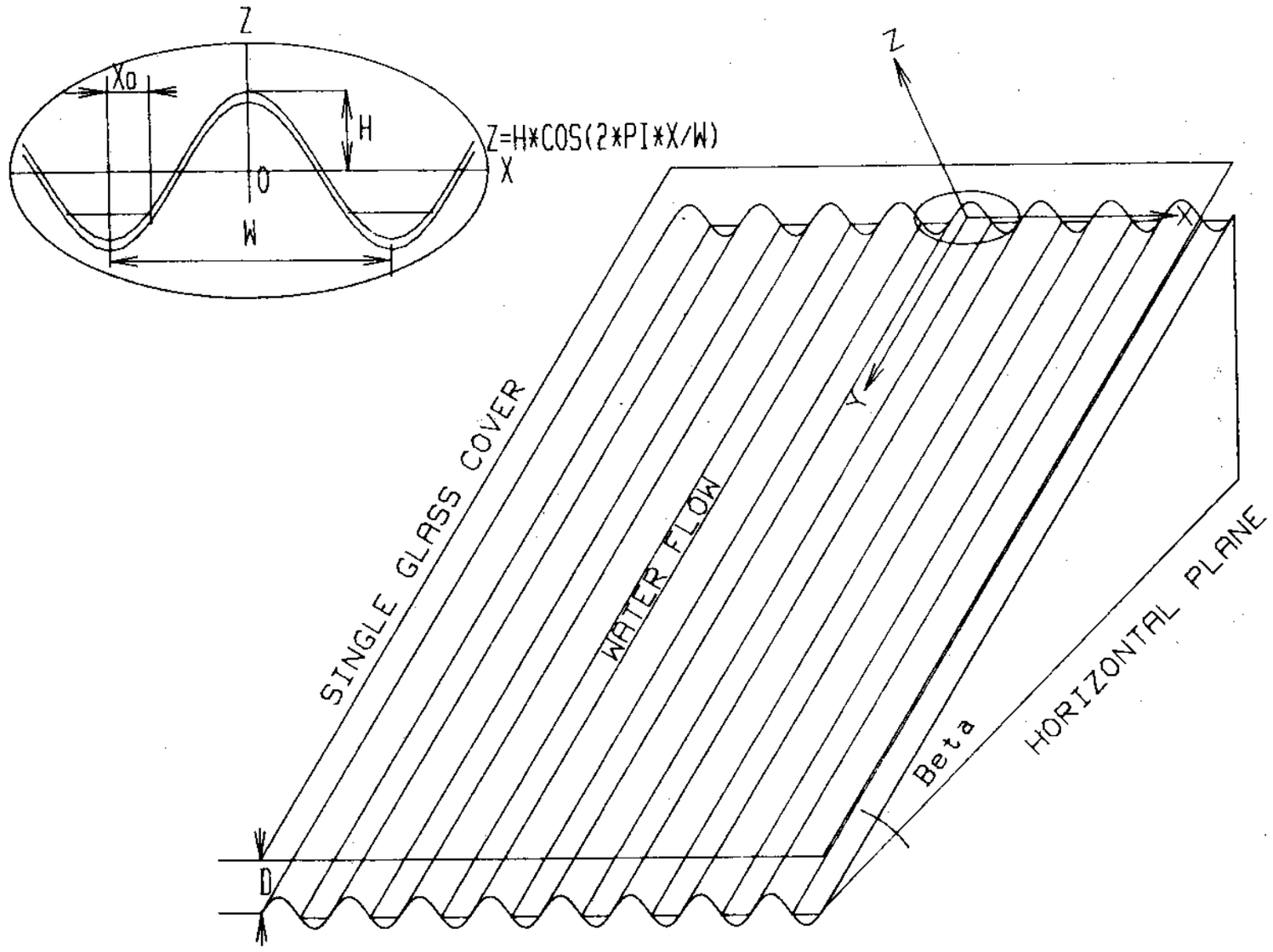

Fig. 1 Overall specification of trickle collector

flat and evaporation can occur and condense on the glazing. The shape of the cross section is one of the principal design factors. Since the most common shape of roof material in Korea is sinusoidally corrugated slate, we selected the cross-sectional shape to be sinusoidal to reduce cost and complexity. In this case, the solar incident angle varies across the corrugation of the absorber surface.

2.1 *Geometrical consideration*

Figure 1 shows the mathematical approximation of the absorber plate and the coordinate system. The displacement of the absorber from the mid-plane is approximated as

$$z = H \cos\left(\frac{2\pi x}{2}\right), \tag{1}$$

where H is the distance to the highest point from the centerline and w is the wavelength.

To simplify the equations, the following non-dimensional parameters are defined:

$$\phi = \frac{H}{w}, \tag{2}$$

$$x^* = \frac{x}{w}, \tag{3}$$

$$x_0^* = \frac{x_0}{w}. \tag{4}$$

2.2 *Fluid flow along the corrugation*

The wetted perimeter and cross-sectional area of fluid vary with the flowrate of the water. Manning's formula[9] for an open channel is adopted for the analysis of fluid motion along the flow channels. Manning's formula is applicable for turbulent flow conditions where the Reynolds number is greater than 2000. Turbulent flow is generally experienced unless the flow rate is very small.

Manning's formula states that

$$V = \frac{C_m}{n} \cdot R^{2/3} \cdot \theta^{1/2}, \tag{5}$$

where V is the mean velocity of fluid, C_m is a conversion factor equal to 1 in SI units, n is a roughness factor depending on the surface condition, θ is equal to sine of the collector tilt angle and R is the hydraulic radius defined by

$$R = A/P. \tag{6}$$

The flow rate Q is then given by

$$Q = A \cdot V \tag{7}$$

where A is flow cross-sectional area and P is the wetted perimeter depending on surface configuration.

For the geometry of the corrugated absorber plate, the above parameters can be easily rewritten as follows:

$$\theta = \sin \beta, \tag{8}$$

$$A = wH \left\{ \frac{1}{\pi} \sin(2\pi x_o^*) - 2x_o^* \cos(2\pi x_o^*) \right\}, \tag{9}$$

$$\rho = 2w \int_0^{x_o^*} \sqrt{1 + (2\pi\phi)^2 \sin^2(2\pi\xi)}\, d\xi, \tag{10}$$

where ξ is a dummy variable.

Figure 2 displays the physical variations of the dimensionless area ($A^* = A/(w^*H)$), perimeter (P^* = P/w), and radius ($R^* = R/H$) with respect to the change of the dimensionless distance x_i^*. Figure 3 shows the variation of the dimensionless flow rate and velocity where the velocity, V^*, and flow rate, Q^*, are defined by

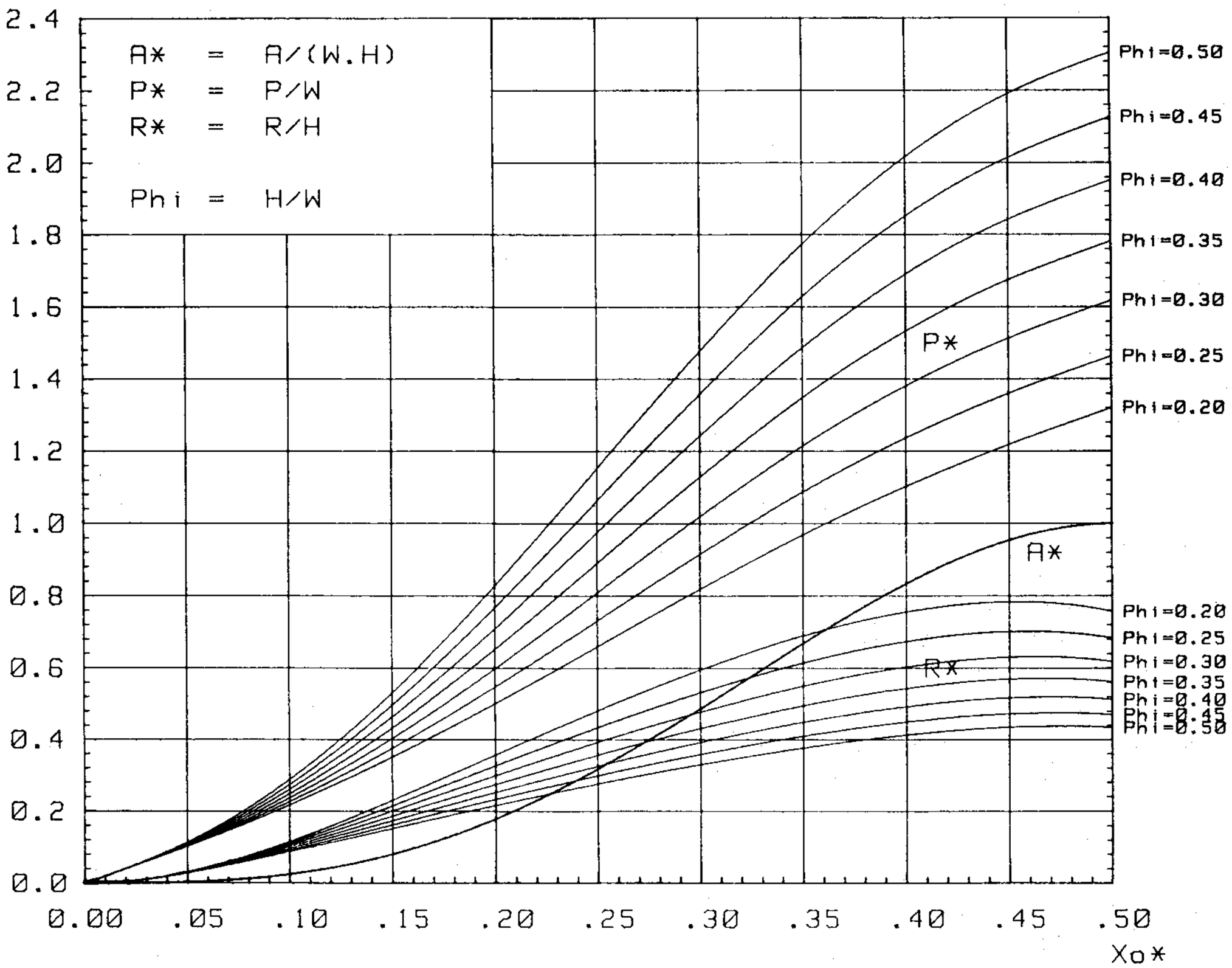

Fig. 2 Variation of A, P, R with respect to X_o.

$$V^* = \frac{n \cdot H^{-2/3}}{C_m \cdot \theta^{1/2}} \cdot V, \tag{11}$$

$$Q^* = \frac{n \cdot w^{-1} \cdot H^{-5/3}}{C_m \cdot \theta^{1/2}} \cdot Q. \tag{12}$$

Finally, a transcendental equation to find x_o for specified flow rate, Q, is setup using eqn (7) to give

$$f(x_o) = \frac{C_m \cdot A^{5/3}}{n \cdot P^{2/3}} \cdot \theta^{1/2} - Q = 0. \tag{13}$$

2.3 *Solar radiation*

2.3.1 *Absorbed radiation*

Since the absorber plate is not flat, the absorbed radiation, S, varies along the x direction. If one considers that the absorbtance of the collector plate is independant of the incident angle, the absorbed solar energy per unit area can be expressed as

$$S(x) = I_b \cdot R_b(x) \cdot (\tau\alpha)_b + I_d \cdot (\tau\alpha)_d \cdot \frac{(1 + \cos\beta)}{2} + \rho_g (I_b + I_d)\,(\tau\alpha)_g \cdot \frac{(1 - \cos\beta)}{2}, \quad (14)$$

where R_b is the ratio of the average beam radiation on the tilted surface to that on a horizontal surface.

2.3.2 *Solar beam analysis*

It is quite convenient to use the unit vectors defined in Fig. 4 to calculate the incident angle of the solar irradiance on the absorber. The component of the characteristic unit vectors, $\vec{U}_1$, $\vec{U}_2$, $\vec{U}_3$ are

$$\vec{U}_1 = \sin\gamma\vec{i} + \cos\gamma\vec{j} \quad (15)$$

$$\vec{U}_2 = -\cos\beta\cos\gamma\vec{i} + \cos\beta\sin\gamma\vec{j} + \sin\beta\vec{k}, \quad (16)$$

$$\vec{U}_3 = U_1 \times U_2 = \cos\gamma\sin\beta\vec{i} - \sin\gamma\sin\beta\vec{j} + \cos\beta\vec{k}. \quad (17)$$

Using these unit vectors and geometrical shape of the cross section of the absorber, the characteristic unit vector, $\vec{U}$, can be determined as a function of x for the given specifications of the collector. The angle α in Fig. 5 is

$$\tan\alpha = \frac{dz}{dx} = -2\pi\phi\sin(2\pi x^*), \quad (18)$$

$$\cos\alpha = \frac{1}{\sqrt{1 + 4\pi^2\phi^2\sin^2(2\pi x^*)}}, \quad (19)$$

$$\sin\alpha = \frac{-2\pi\phi\sin(2\pi x^*)}{\sqrt{1 + 4\pi^2\phi^2\sin^2(2\pi x^*)}}. \quad (20)$$

Since $\vec{U}$ must satisfy following equations:

$$\vec{U}\cdot\vec{U}_2 = 0, \quad (21)$$

$$\vec{U}\cdot\vec{U}_3 = \cos\alpha, \quad (22)$$

$$\vec{U}\cdot\vec{U}_1 = -\sin\alpha, \quad (23)$$

we obtain

$$\vec{U} = (\cos\alpha\sin\beta\cos\gamma - \sin\alpha\sin\gamma)i$$

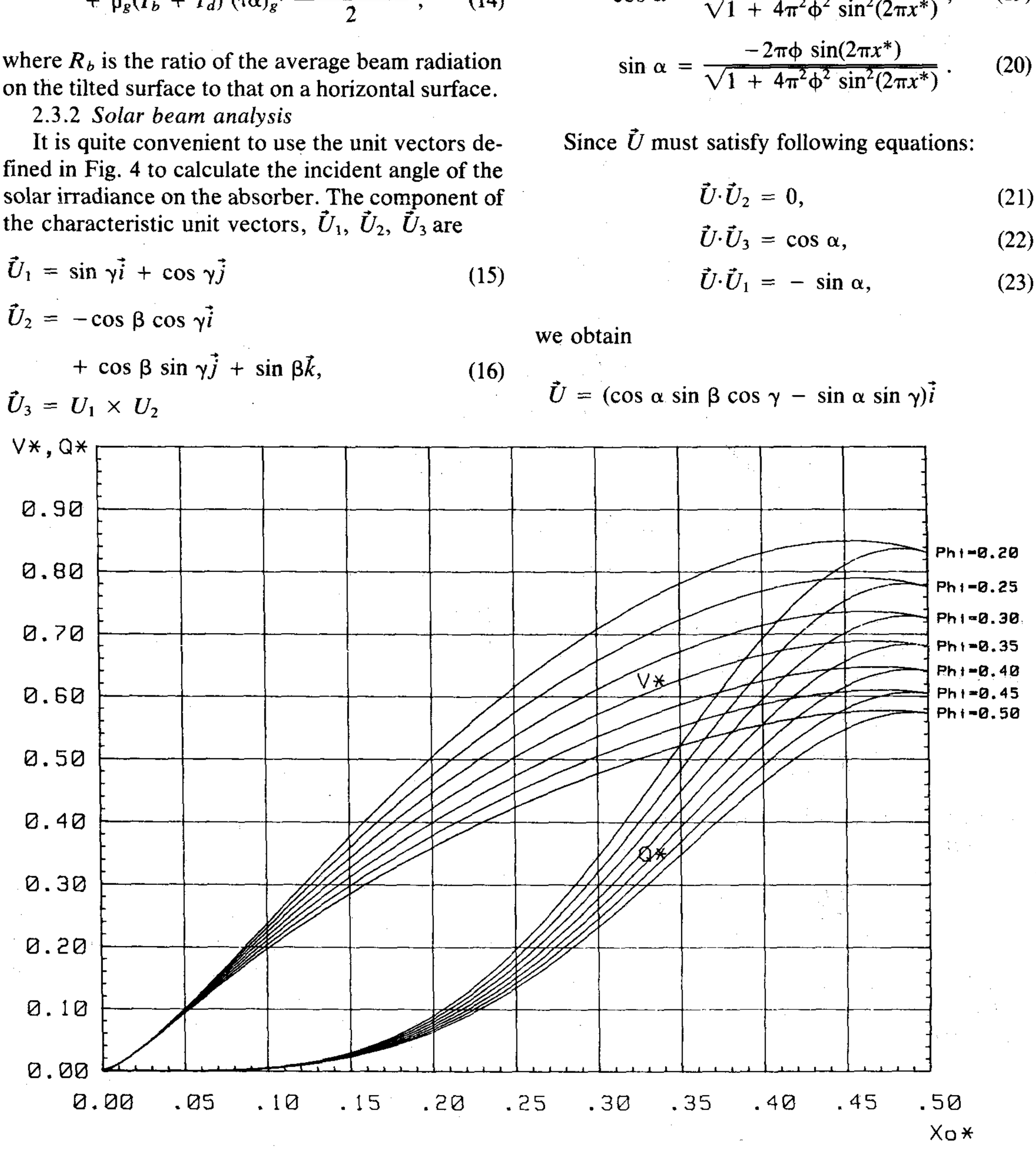

Fig. 3 Variation of V^*, Q^* with respect to X_o^*

$$- (\cos\alpha \sin\beta \sin\gamma + \sin\alpha \cos\gamma)\vec{j}$$
$$+ \cos\beta \cos\alpha\vec{k}. \quad (24)$$

The solar beam vector, $\vec{S}$, is expressed as

$$\vec{S} = (\sin\psi \cos\omega \cos\delta - \cos\psi \sin\delta)\vec{i}$$
$$- \cos\delta \sin\omega\vec{j}$$
$$+ (\cos\delta \cos\psi \cos\omega + \sin\delta \sin\psi)\vec{k}, \quad (25)$$

where ψ is the latitude, ω is the hour angle to be calculated from the day of the year and γ, δ, β are the surface azimuth angle, declination and slope angle, respectively.

Since the corrugated absorber partially shades itself as shown Fig. 5, it is important to calculate

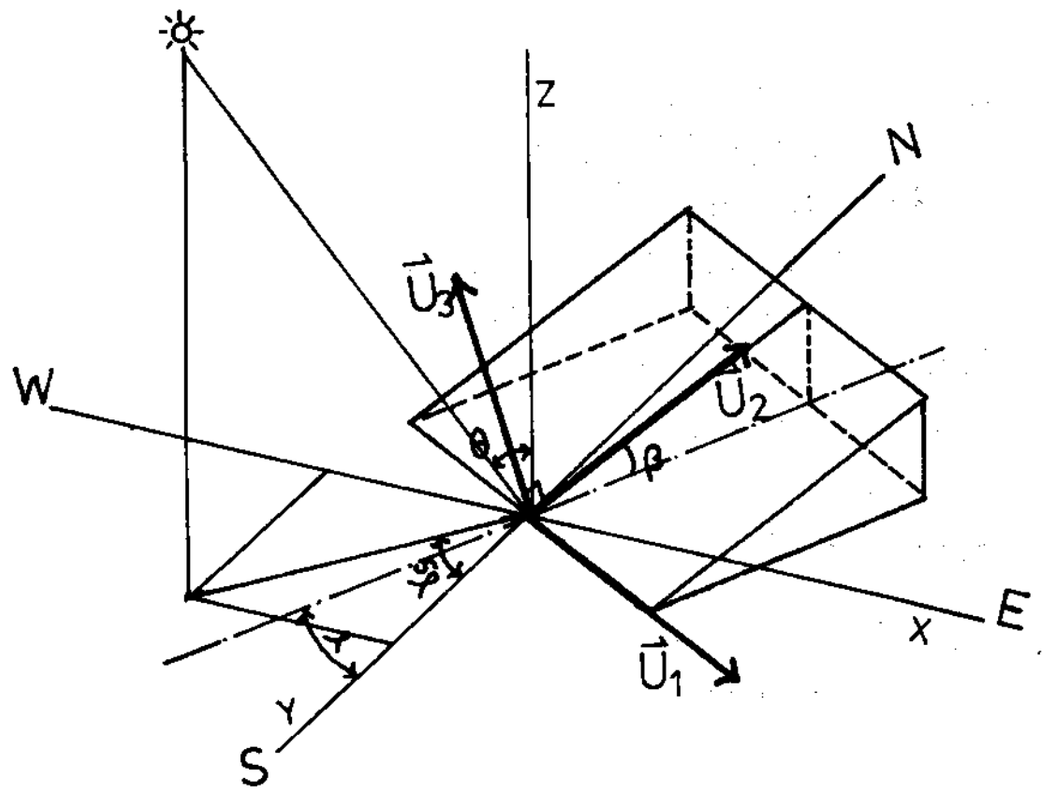

Fig. 4 Collector position and characteristic vectors

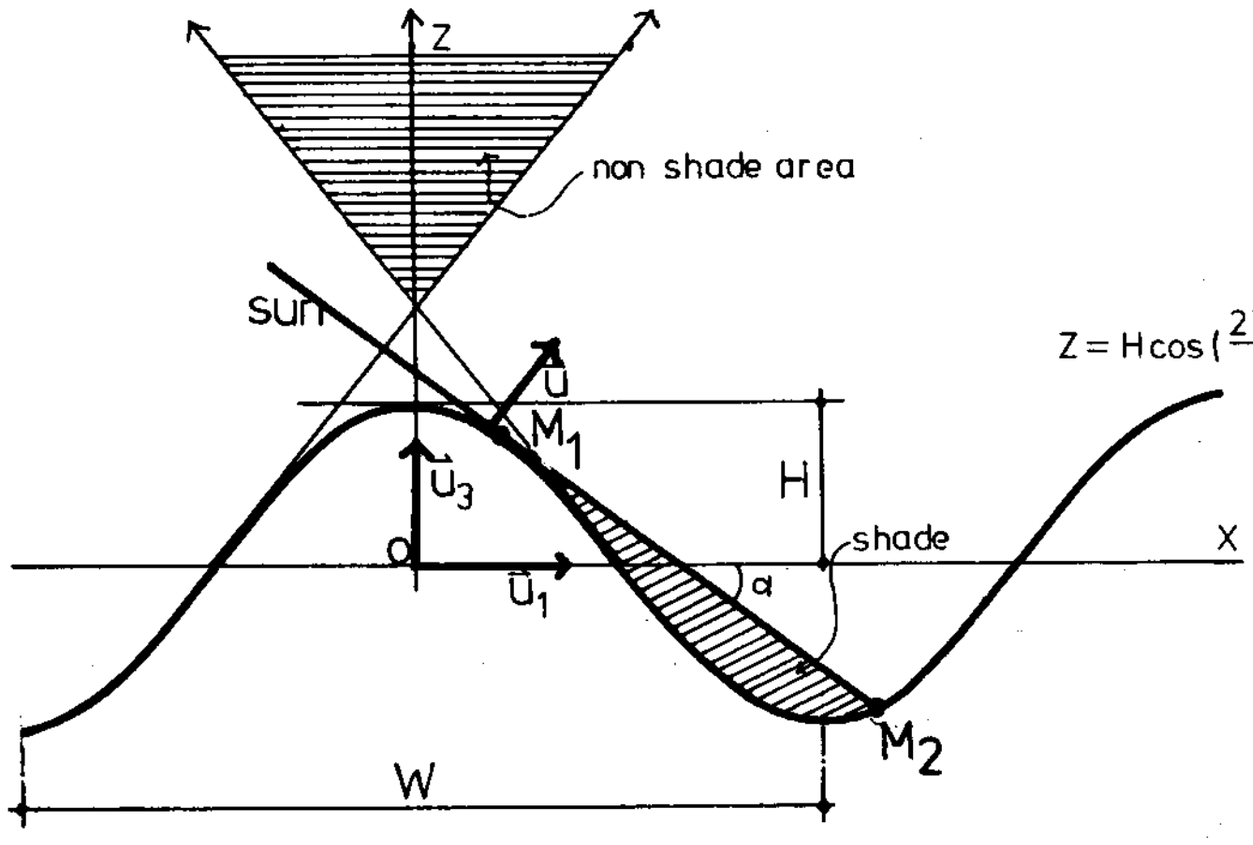

Fig. 5 Cross-sectional view of absorber

the shaded region on the absorber for the analysis of the incident beam radiation. This can be expressed by the following two equations. If

$$\left| \frac{\vec{S}\cdot\vec{U}_3}{\vec{S}\cdot\vec{U}_1} \right| \geqslant \frac{2\pi H}{w}, \quad (26)$$

then none of the absorber plate is shaded by itself. However, when

$$\left| \frac{\vec{S}\cdot\vec{U}_3}{\vec{S}\cdot\vec{U}_1} \right| < \frac{2\pi H}{w}, \quad (27)$$

there is some self-shading of the absorber plate. Under these conditions the X coordinate of the two limit points, M_1 and M_2 in Fig. 5, on the absorber are given by

$$x_1 = \frac{w}{2\pi} \sin^{-1}\left(- \frac{w}{2\pi H} \cdot \frac{\vec{U}_3\cdot\vec{S}}{\vec{U}_1\cdot\vec{S}} \right), \quad (28)$$

$$\frac{\vec{U}_3\cdot\vec{S}}{\vec{U}_1\cdot\vec{S}} (x_2 - x_1)$$
$$= H \left\{ \cos\left(\frac{2\pi}{w} \cdot x_2\right) - \cos\left(\frac{2\pi}{w} \cdot x_1\right) \right\}. \quad (29)$$

Finally, $R_b(x)$ is expressed merely as

$$R_b(x) = [\vec{S}\cdot\vec{U}]^+. \quad (30)$$

The meaning of the + exponent is that only positive values of the terms in the square bracket are meaningful (it is zero if the term is negative), and the split of total solar radiation on a horizontal surface into its diffuse component and beam component is determined using Orgill and Holland's correlation[10].

2.4 *Temperature distribution on the absorber*

From Fig. 6, assuming no plate conduction in the direction of flow, the energy balance equation

on absorber plate is given by

$$k\,\delta\,\frac{d^2T}{dl^2} + S(x) - U_t(T - T_a) = 0 \qquad (31)$$

It is convenient to transform the l-coordinate system into the x-coordinate system. The coordinate transformation operators are

$$Z' = \frac{dz}{dx}, \qquad (32)$$

$$Z'' = \frac{d^2z}{dx^2}. \qquad (33)$$

The heat transfer equation then becomes

$$\frac{d^2T}{dx^2} - \frac{Z''\cdot Z'}{1 + Z'^2}\cdot\frac{dT}{dx} + \frac{(1 + Z'^2)(S(x) - U_L(T - Ta))}{k_p\cdot d_p} = 0. \qquad (34)$$

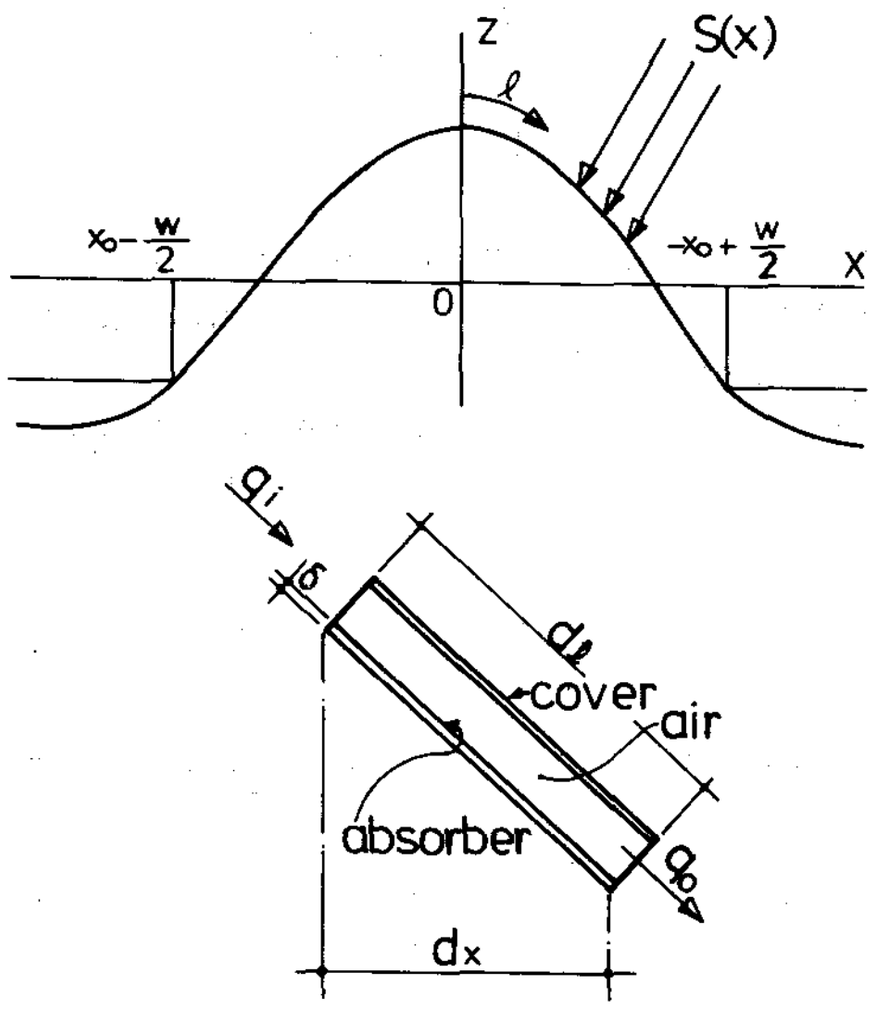

Fig. 6 Heat conduction in the absorber

If one consider that the fluid temperature of the each section is uniform and the temperature of the boundary condition are equal to the fluid temperature, we have the following boundary conditions:

$$T\left(\frac{w}{2} + x_0\right) = T_f(y), \qquad (35)$$

$$T\left(\frac{w}{2} - x_0\right) = T_f(y). \qquad (36)$$

In addition at each vertical position, y_0, the variation of the relative temperature in the X direction was assumed to be only a function of X so that one can define $T_0^*(x)$ as

$$T_0^*(x, y_0) = T(x, y_0) - T_f(y_0) \qquad (37)$$

and after rearranging the governing equation, one obtains

$$\frac{d^2T_0^*}{dx^2} - \frac{Z'\cdot Z''}{1 + Z'^2}\cdot\frac{dT_0^*}{dx} + \frac{(1 + Z'^2)U_L}{k_p\cdot d_p}\left\{\frac{S(x)}{U_L} - (T_0^* + T_{f0} - T_a)\right\} = 0. \qquad (38)$$

The boundary conditions then become

$$T_0^*\left(\frac{w}{2} + x_0\right) = 0, \qquad (39)$$

$$T_0^*\left(\frac{w}{2} - x_0\right) = 0. \qquad (40)$$

2.5 *Fluid temperature*

2.5.1 *Simplified assumptions*

The major assumptions are:

(1) Performance is steady state.

(2) Temperature gradient on absorber is negligible along the y direction and z direction (one-dimensional heat flow along the x direction).

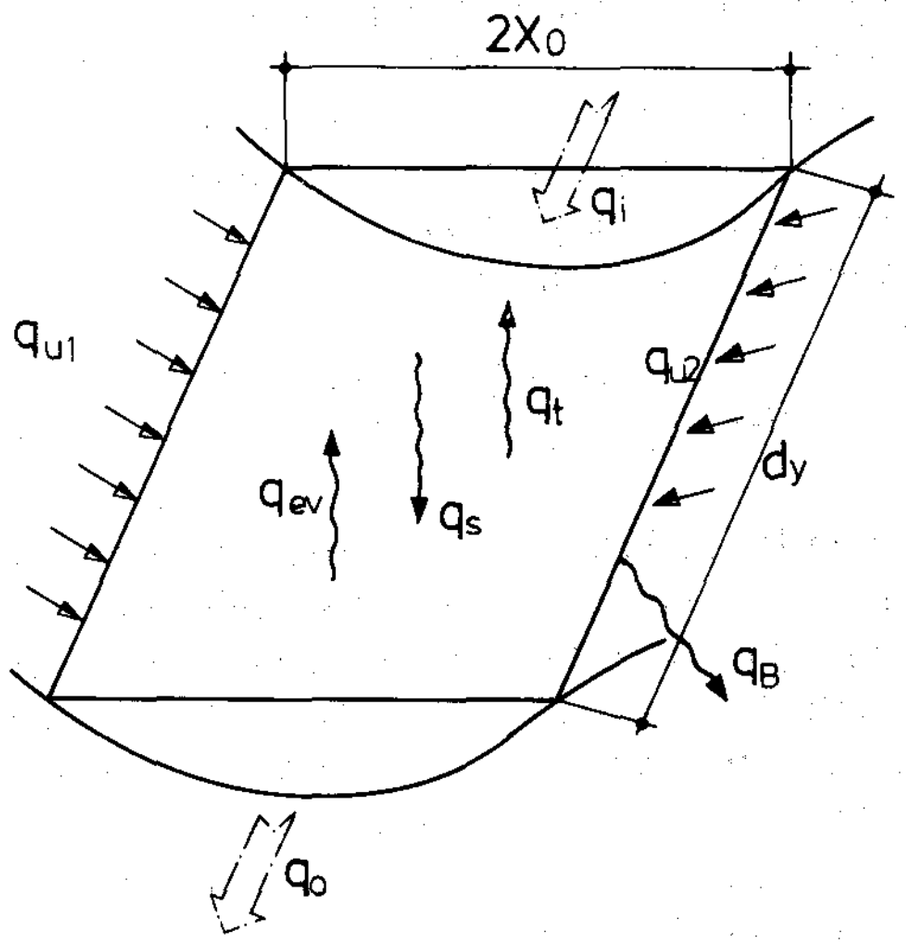

Fig. 7 Energy balance in fluid

(3) Natural convection heat transfer coefficient between the cover and corrugated absorber is the same as that of two inclined isothermal flat plates separated by a distance L.

(4) Flow is uniform.

(5) Boundary conditions at the end of each fin are

at a constant temperature.
(6) Dust on the glazing has a negligible effect.
(7) Edge side loss is neglible.

Figure 7 shows the energy balance on a fluid element. We can express an energy balance on the fluid flowing through a single channel as

$$q_{u1} + q_{u2} + q_s + q_i - q_o - q_{ev} - q_t - q_B = 0. \quad (41)$$

Therefore

$$\frac{dT_f}{dy} + \frac{2U_L \cdot x_0}{\rho \cdot Q \cdot C_f}(T_f - T_a) - \frac{S_f}{\rho \cdot Q \cdot C_f} - \frac{k_p \cdot d_p}{\rho \cdot Q \cdot C_f} \cdot \frac{dT}{dx} \cdot \frac{1}{\sqrt{(1 + z'^2)}} \Bigg|_{w/2 - x}^{-w/2 + x} + \frac{q_{ev}}{\rho \cdot Q \cdot C_f} + \frac{q_t}{\pi \cdot Q \cdot C_f} + \frac{q_B}{\rho \cdot Q \cdot C_f} = 0, \quad (42)$$

where C_f is the specific heat of the fluid. S_f, the overall useful solar radiation received on the fluid surface, can be found as

$$S_f = (1 - \rho_f) \int_{-w/2 + x_o}^{w/2 - x_o} S(x) \cdot dx, \quad (43)$$

where ρ_f is the reflectance of the fluid.

Determining the latent heat transfer from the evaporation/condensation process in eqn (41) is complicated by the convection and radiation heat transfer processes. A very simple equation in Refs. (4)–(6) has been used here to estimate the evaporation/condensation related heat transfer losses from the surface of a fluid,

$$q_{ev} = \frac{D_{dv} \cdot P}{L_{cv} \cdot R_{cv} \cdot T_f} \cdot \ln\left(\frac{P - P_{cp}}{P - P_{pp}}\right) h_{fc}, \quad (44)$$

where P_{pp} and P_{cp} are the partial pressures of water vapor at the temperature of the collector plate and inner glazing surface, respectively. The diffusion length, L_{cv}, is the distance between the glazing surface and the water surface (valley of the corrugated plate). The diffusion coefficient of water vapor in air, D_{dv}, is 2.55×10^{-5} m^2/s. h_{fc} and R_{cv} are the latent heat of evaporation of fluid and the universal gas constant, respectively.

2.5.2 *Detailed calculation of heat transfer coefficient*

The convective heat transfer between the cover and corrugated plate can be expressed as

$$h_{con} = \frac{N_{u \cdot k}}{L}. \quad (45)$$

The Nusselt Number, N_u, can be expressed as reported by Hollands *et al.*[11]

$$N_u = 1 + 1.44\left(1 - \frac{1708}{R_a \cdot \cos\beta}\right)^+ \times \left(1 - \frac{(\sin 1.8\beta)^{1.6} \times 1708}{R_a \cdot \cos\beta}\right)^+ + \left[\left(\frac{R_a \cdot \cos\beta}{5830}\right)^{1/3} - 1\right]^+, \quad (46)$$

where the term within $[\ ]^+$ is set equal to zero if its value is negative. The Rayleigh number, R_a, is defined as

$$R_a = \frac{g\beta' \Delta T L^3}{\nu \cdot \alpha}. \quad (47)$$

The basic equation for the radiative transfer between the cover and corrugated plate is

$$h_{r,c} = \frac{\sigma(T_2^2 + T_1^2)(T_2 + T_1)}{\frac{1 - \epsilon_1}{\epsilon_1 + 1} + \frac{1}{F_{1,2}} + \frac{(1 - \epsilon_2)A_1}{\epsilon_2 \cdot A_2}}, \quad (48)$$

where ϵ_1 is the absorber emissivity, ϵ_2 is the plate emissivity, A_1, A_2 are the surface area and F is the view factor.

It is evident from Fig. 8 that one may approximate $A_1 = A_3$ and $F_{1,2}$ can be expressed as

$$F_{1,2} = 1 - F_{1,1} = \sin\frac{\Omega}{2}. \quad (49)$$

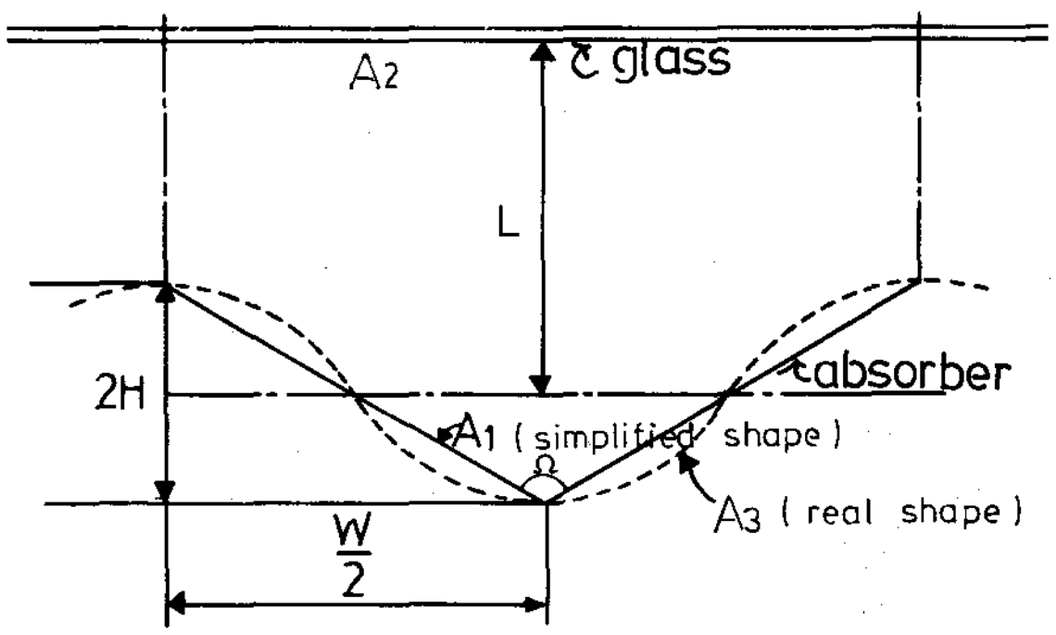

Fig. 8 Calculation of view factor

The convective transfer coefficient for collectors[10] is wind dependent and can be expressed as

$$h_w = 5.7 + 3.8V_w, \quad (50)$$

where V_w is the wind speed.

The radiative heat transfer coefficient between the sky and the cover is

$$h_{r,\mathrm{sk}} = \sigma \cdot \epsilon_2 (T_{\mathrm{sk}}^2 + T_c^2)(T_{\mathrm{sk}} + T_c), \quad (51)$$

where the sky temperature is given by

$$T_{\mathrm{sk}} = 0.0552 T_a^{1.5}. \quad (52)$$

Finally the overall heat transfer coefficient from the corrugated surface to the ambient can be described as

$$U_L = U_t + U_B, \quad (53)$$

$$U_t = \frac{1}{\dfrac{1}{h_{r,c} + h_{\mathrm{con}}} + \dfrac{1}{h_{r,\mathrm{sk}} + h_w}}, \quad (54)$$

$$U_B = \frac{k_B}{d_B}, \quad (55)$$

where k_B is the conductivity of the back side insulation and d_B is the back side insulation depth.

2.5.3 *Numerical calculation*

For the analysis the absorber plate is divided into equal segments in the direction of the water flow (with each segment having sections), considered as curved fins with hypothetical adiabatic cuts between them. At the entrance of the collector the temperature distribution on the first fin can be solved using the Runge Kutta method assuming constant boundary temperature. On the second node it is possible to determine the fluid temperature using the temperature distribution obtained on the first node. Following the same steps until the last node, the temperature distribution on the whole absorber can be determined.

3. EXPERIMENTAL AND THEORETICAL RESULTS

Two different collector systems were tested. One is the open type and the other is closed type. The open type has four vents (3 cm × 15 cm each) at the bottom and at the top of the collector frame between the absorber and glass cover, while the closed type does not have vents. Here the theoretical analysis was performed using the closed type model. Since the collector can be damaged from the high stagnation temperature, it is important to prevent collectors from overheating. In order to meet this requirement, openings were adopted to enhance the natural convective cooling of the absorber plate of the collector.

3.1 *Experimental appartus*

The prototype models for the tests are with the following specifications.

(1) Effective solar collection area: 5 m^2.
(2) Absorber plate: flat-black paint on an aluminum plate.
(3) Plate thickness: 1 mm.
(4) Glazing: single low-iron glass (3 mm thick).
(5) Aspect ratio (H/w): 0.15. (a) Height: 0.01 m. (b) Corrugation width: 0.065.
(6) Tilted angle: 30°.
(7) Flow rates: 250, 300 and 350 l/h.

In order to control the fluid flow precisely, the main valve is installed ahead of the pump, and subsidiary valves for supplying the same water flow to each solar collector are used. A float valve is also used for maintaining the water height in storage tank. Each flow of solar collector is controlled manually. The solar radiation is measured with the Eppley Precision Spectral Pyranometer, and the inlet and outlet temperature of water, the temperature of the absorber plate, glass cover and ambient are measured with T-type thermocouples.

The temperature measurement location on the absorber plate and glass cover, presented in Fig. 9, were selected for finding thermal distribution in the normal direction of water flow. Thermocouples were also arranged in horizontal direction. The temperature of glass cover is measured on the outside surface of the glass cover. The output voltage from the pyranometer and thermocouples are collected through a Data Aquisition & Control system. Using a computer as a controller, all data are automatically analyzed for the efficiencies, etc.

3.2 *Efficiency of solar collector*

For outside test condition, it is very difficult to maintain constant design conditions (radiation, flow, exit and entrance temperature, etc.). Therefore the data are integrated and integral average values are used in the analysis.

The efficiency of solar collector is defined as follows:

$$E = \frac{\displaystyle\int_{t_{\mathrm{st}}}^{t_{\mathrm{et}}} Q \cdot C_p \cdot \Delta T \cdot \mathrm{d}t}{\displaystyle\int_{t_{\mathrm{st}}}^{t_{\mathrm{et}}} I \cdot \mathrm{d}t}, \quad (56)$$

where t_{st} is the start time of the measurement, t_{et} is the end time of the measurement, ΔT is the water temperature difference between exit and entrance of the solar collector and I is the total insolation on the solar collector surface. $\bar{T}_{fi}$, the average inlet

temperature is also defined:

$$\bar{T}_{fi} = \frac{\int_{t_{st}}^{t_{et}} \cdot T_{fi} \cdot \mathrm{d}t}{t_{et} - t_{st}} . \qquad (57)$$

In the same manner, $\bar{T}_a$, the average ambient temperature and $\bar{T}_{fo}$, the average outlet temperature can be integrated.

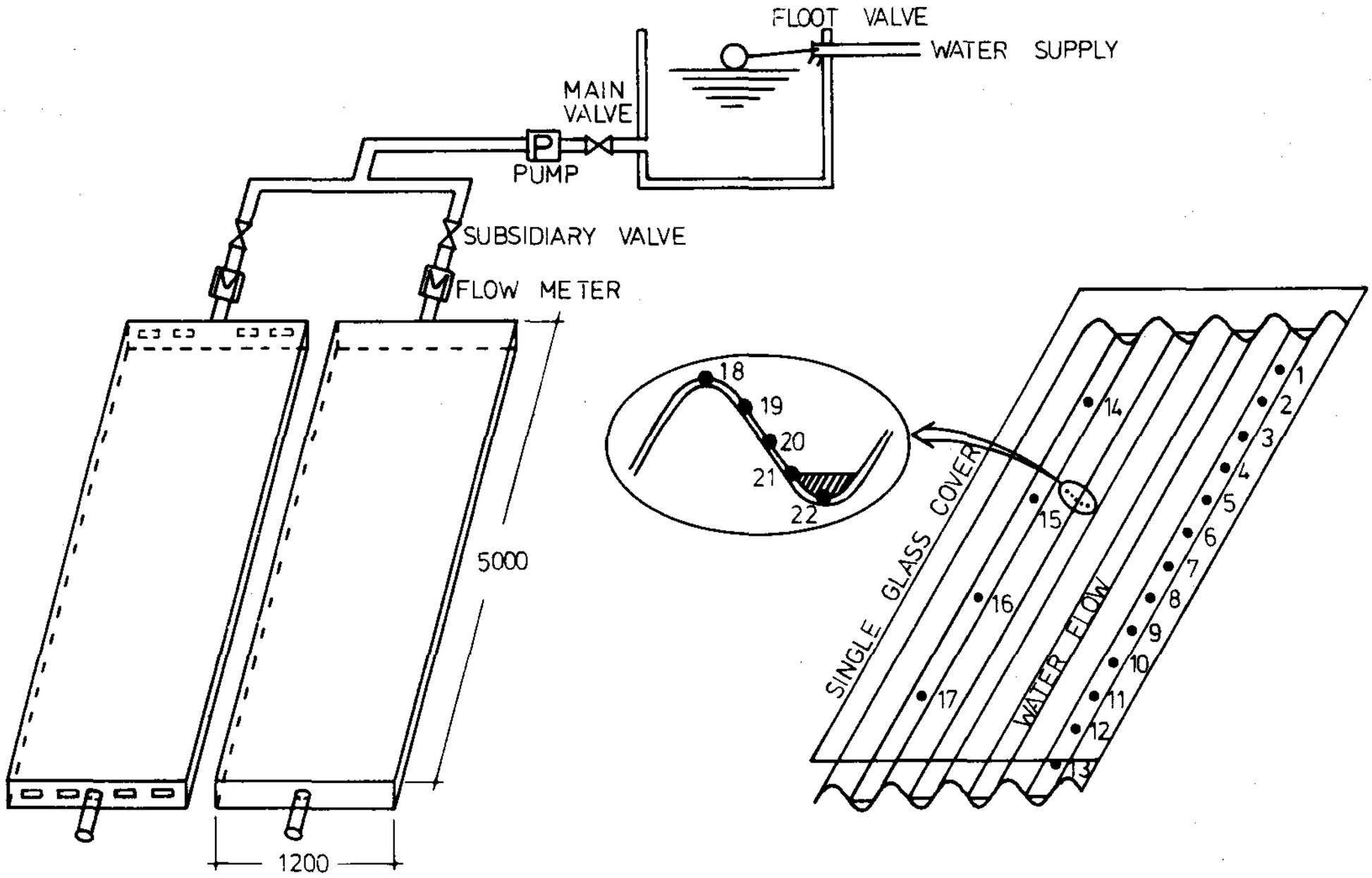

Fig. 9 Schematic diagram of the experimental apparatus

3.3 *Results and discussions*

Table 1 shows the experimental and theoretical results for the closed type collector from September to November 1983. Here T_a and T_{fi} are the ambient temperature and the inlet fluid temperatures, T_o and T_{oc} are the actual outlet fluid temperature and the calculated outlet fluid temperatures, respectively. The measured and the calculated efficiencies of the collector are represented by E_{fe} and E_{fc}. For the system designed to operate with a $(T_o - T_a)/I$ around 0.02 cm^2/W, the measured collector efficiency was approximately 60%. The agreement between the experimental and the theoretical results appears to be reasonable. The temperature differences between T_o and T_{oc} were less than 1°C, while the differences between E_{fe} and E_{fc} are less than 5–10%. However, for higher inlet fluid temperatures and for larger temperature differences between inlet and outlet fluid temperature, the actual collector efficiencies were less than those of calculated values with the differences between E_{fe} and E_{fc} being as much as 15%. This may be caused by the higher condensation and evaporation losses between the absorber and the glazing of the collector. The influence of condensate droplets on the transmittance of incident solar energy was studied both experimentally and analytically by Beard *et al.* (4–6). A 10–15% reduction in solar energy transmittance was observed experimentally by Beard when water droplets formed on the glass inner surface.

Least squares fitting of computed and experimental data for the closed collector give the following efficiency equation.

(a) Calculated efficiency

$$E_{fc} = 0.803 - 8.04(T_{fi} - T_a)/I. \qquad (58)$$

(b) Experimental efficiency

$$E_{fe} = 0.787 - 10.822(T_{fi} - T_a)/I. \qquad (59)$$

Figure 10 also shows the comparisons between the experimental and the theoretical collector efficiencies for the closed type and the experimental collector efficiency for the open type. As would be expected, the efficiency of the open type was lower than that of the closed type.

The experimental efficiency equation of the

open type collector was found to be

$$E_{fe} = 0.781 - 14.327(T_{fi} - T_a)/I. \quad (60)$$

At the small temperature differences between inlet and outlet fluid temperature, the overall performance of the open type collector is decreased slightly; however, at the high temperature differences, the performance of the open type collector is decreased a lot. The openings can provide the benefit of eliminating the condensation. However, the evaporation and infiltration losses appears to be

Table 1 Experimental and theoretical results

Solar radiation $I(W/m^2)$	Ambiant temperature $T_a(C)$	Inlet fluid temperature $T_{fi}(C)$	Measured outlet fluid temperature $T_o(C)$	Calculated outlet fluid temperature $T_{oc}(C)$	Measured collector efficiency $E_{fe}(\%)$	calculated collector efficiency $E_{fc}(\%)$
845	25.7	24.6	34.4	34.5	80.9	81.9
865	26.7	24.7	36.5	37.0	79.4	82.7
635	26.6	24.7	31.0	31.2	81.0	83.2
862	26.1	37.1	45.8	46.0	70.4	71.7
990	28.2	55.1	61.0	62.8	47.0	61.3
983	29.0	57.0	63.5	65.5	46.0	60.3
959	29.3	38.9	49.0	49.0	73.7	73.7
841	25.7	30.3	39.2	39.6	73.9	77.0
911	26.5	40.1	48.5	49.3	64.2	70.2
1,022	27.6	40.0	50.1	50.6	69.0	72.2
1,073	19.9	52.8	59.6	61.9	44.0	58.8
1,017	20.9	44.7	53.0	54.0	57.2	64.0

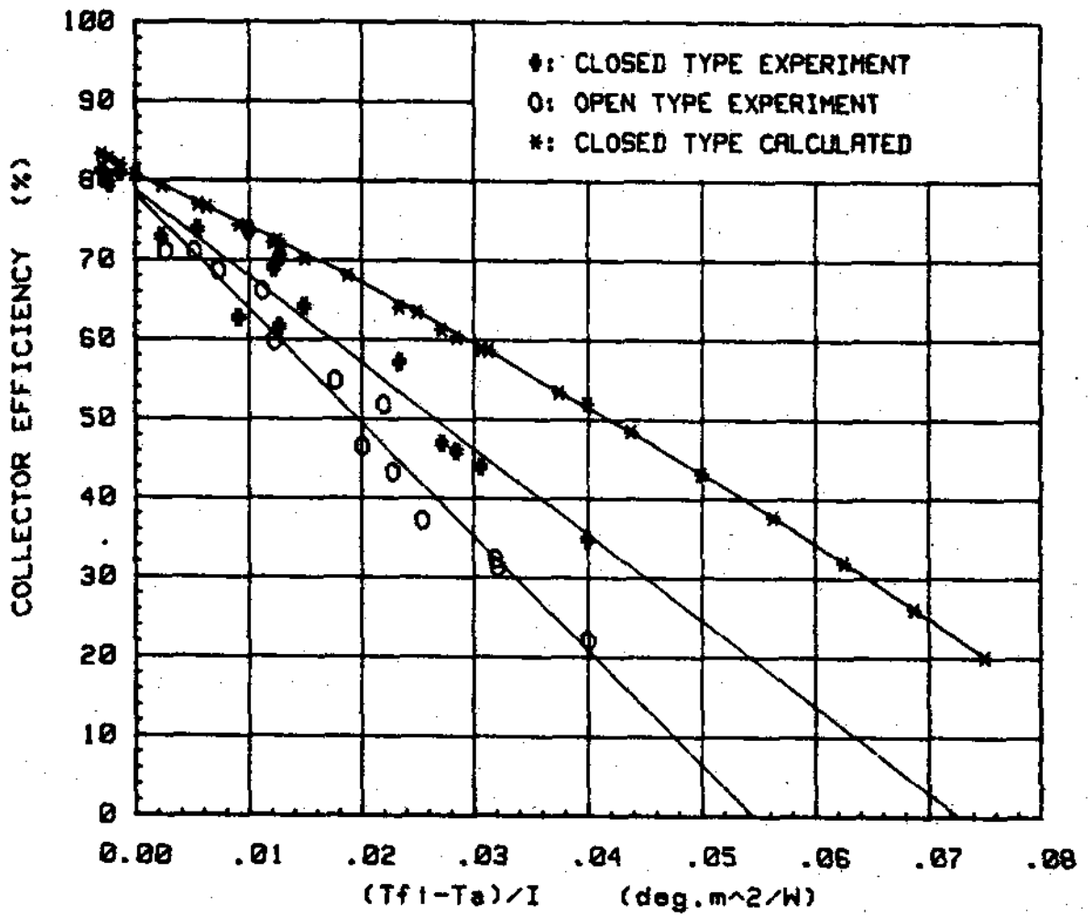

Fig. 10 Comparison of collector efficiencies

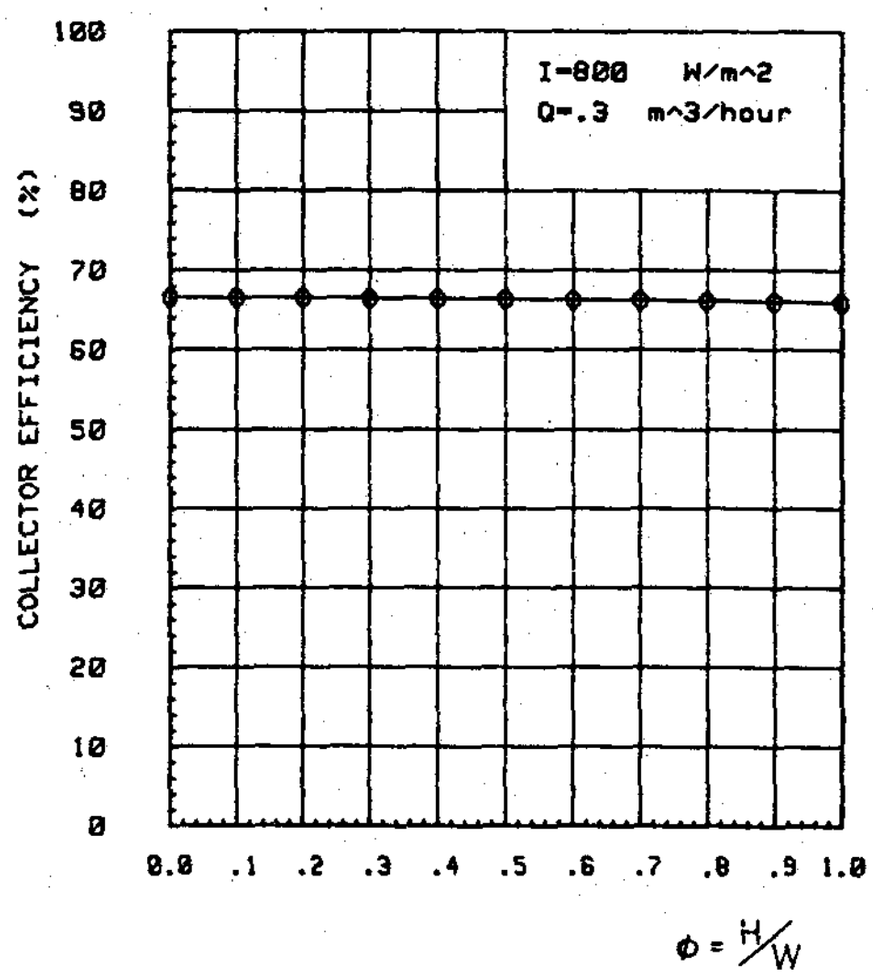

Fig. 11 Effect of aspect ratio on efficiency

significant in the collector at the high temperature differences. A detailed study such as fogging, evaporation, condensation on the cover plate and infiltration losses, both open type and closed type, may be needed to quantitatively correct the deviations between the experimental and the theoretical analysis for the higher fluid inlet temperature and for larger temperature increase.

Actually the open type system is simpler to maintain. This may be a significant advantage over the closed type in spite of a large decrease in the overall performance at the high temperature differences between inlet and outlet fluid temperature. Many practical solar systems, for example, swimming pool heating, industrial preheat systems, etc., would operate at small temperature differences between the inlet and outlet fluid temperature.

The influence of design modifications on the collector performance were also studied using the theoretical model. The aspect ratio (H/w) is shown in Fig. 11 to have little effect on the collector efficiency as long as w is not extremely large. Higher flow rates increase the efficiency through reduction in conduction distance. It is needless to say that the high flowrates also lead to lower losses since average temperature is lower. Distance between the corrugation has a weak effect on the efficiency. Varying other variables such as irradiation, ambient temperature, collector tilt, wind speed and plate to glazing spacing led to almost the same results as that of Refs. (4), (5) and (6).

NOMENCLATURE

- d thickness
- E efficiency
- g gravitational constant
- h heat transfer coefficient
- I solar radiation
- k thermal conductivity
- L mean distance between absorber plate
- p wetted perimeter in eqns (6) and (13), pressure in eqn (44)
- q heat loss
- t time
- T temperature

$T_f(y_o) = T_{fo}$

- U unit vector
- U heat loss coefficient
- α absorptance in eqn (14), angle from eqn (18) to eqn (24), thermal diffusivity in eqn (47)
- β volumetric coefficient of expansion in eqn (47), slope angle from eqn (14) to eqn (25)
- ν kinematic viscosity
- ρ reflectance, density in eqn (42)
- σ Stefan-Boltzmann constant
- τ transmittance

Subscripts

- a ambient
- b beam
- B bottom
- c cover
- d diffuse
- ev evaporation
- f fluid
- g ground
- i inlet
- L total
- o outlet
- p plate
- r radiation
- S absorbed solar energy
- sk sky
- t top
- $u1$, $u2$ conduction heat transfer
- w wind

REFERENCES

1. R. L. San Martin and G. J. Field, Experimental performance of three solar collectors. *Solar Energy* **17**, 345–349 (1975).
2. P. R. Smith, Numerical modelling of thermal-trap and water-trickle solar collectors. *Proceedings of the Workshop on Solar Collectors for the Heating and Cooling of Buildings*, pp. 315–321. NSF RA N-75-109, New York City, Nov. 21–23, 1974.
3. G. E. Bush, Evaluation of home solar heating system. Lawrence Livermore Laboratory, UCRL-51711, (1975).
4. J. T. Beard *et al.*, Design and operational influences on thermal performance of "Solaris" Solar Collector. The Winter Annual Meeting, Atlanta, Ga., Nov. 27–Dec. 2, 1977 of the A.S.M.E.
5. J. T. Beard *et al.*, Analysis of thermal performance of "Solaris" water-trickle solar collector. Contributed by the Solar Energy Division of the A.S.M.E. for presentation at the Winter Annual Meeting, New York, Dec. 5, 1976.
6. J. T. Beard, Engineering analysis and testing of water-trickle solar collector. Report Nos. 1–3, ORO-4927-76/1, ORO-4927-76/2 and ORO-4927-77/1, Division of Solar Energy, Energy Research and Development Administration, 1976–1977.
7. W. B. May, Jr., Theoretical model of the "Solaris" open water flow solar collector. MS Thesis, University of Virginia, School of Engineering and Applied Science, Charlottesville, Virginia (1977).
8. Wang Shing-An, An experimental study of corrugated steel sheet solar water heater. *Solar Energy*, **23**, 333–341 (1979).
9. V. L. Streeter and E. B. Wylie, *Fluid Mechanics*, 7th ed. McGraw-Hill, New York (1979).
10. J. A. Duffie and W. A. Beckman, *Solar Engineering of Thermal Processes*. John Wiley & Sons, New York (1980).
11. K. G. T. Hollands, T. E. Unny, G. D. Raithby and L. Konicek, Free convection heat transfer across inclined air layers. A.S.M.E. *J. Heat Transfer* **98**, 189–193 (1976).
12. J. Coleman, The site-built trickle collector. ISBN 0-89696-050-1. Solar Age Resource Book, 1133 Avenue of the Americas, N.Y. 10036, Everest House (1979).
13. J. P. Holman, *Heat Transfer*. McGraw-Hill, New York (1976).
14. R. Siegel and J. R. Howell, *Thermal Radiation Heat Transfer*. McGraw-Hill, New York (1972).
15. A. Feingold, Radiant-interchange configuration factor between various selected plane surfaces. *Proc. Roy. Soc. (London), Ser. A* **292**, 51–60 (1966).
16. B. Carnahan, H. A. Luther and J. O. Wilkes, *Applied Numerical Methods*. John Wiley & Sons, New York (1969).
17. J. H. Keenan, F. G. Keys, P. G. Hill and J. G. Moore, *Steam Tables*. John Wiley & Sons, New York .